Feedback gain functions in the Lorenz-63 model

May 2007

Complement to a Letter to Euro.Phys.Lett.
(informal research paper of the TEF-ZOOM collaboration[1]*)*

As a reminder of the famous "butterfly effect"[2], that proves how Poetry, Art and Science together might be the future of mankind...

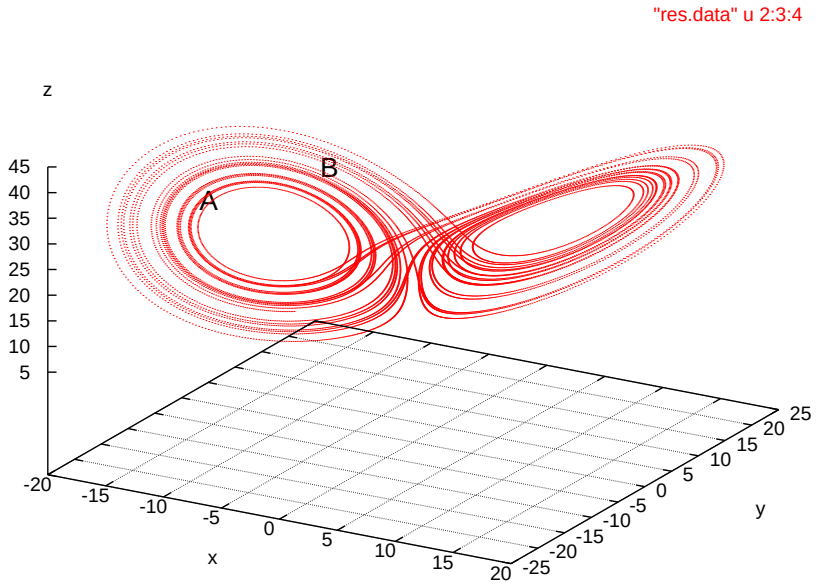

FIG. 1 – The Lorenz attractor.

Referring to the Letter, the only transfer variable here is $\varphi = xy$. This test-variable corresponds to an interaction between the flow intensity and a temperature difference between ascending and descending fluid particles. The original Lorenz system is cast to its feedback-form as follows

$$\begin{cases} \partial_t x = s(y-x) \\ \partial_t y = (rx - y - xz) \\ \partial_t z \ = -bz + xy \end{cases} \quad \overset{Feedback}{\longrightarrow} \quad \begin{cases} \partial_t x = s(y-x) \\ \partial_t y = (rx - y - xz) \\ \partial_t z \ = -bz + \varphi \\ \varphi = xy \end{cases} \tag{1}$$

[1] by Al1 and StepH.

[2] for non climatologist readers, the said "butterfly effect" does not refer to the double wing shape of the Lorenz attractor, but to its chaotic behavior. Is this at the origin of most people describing the attractor as butterfly wings shaped ?

The "nonlinear" feedback effect of the system on φ is computed with the Mini_ker program (see manual in the web pages) using the extension **Psi_t, ko_pert_Type**= 3 activated, and of course is depending on the starting point.

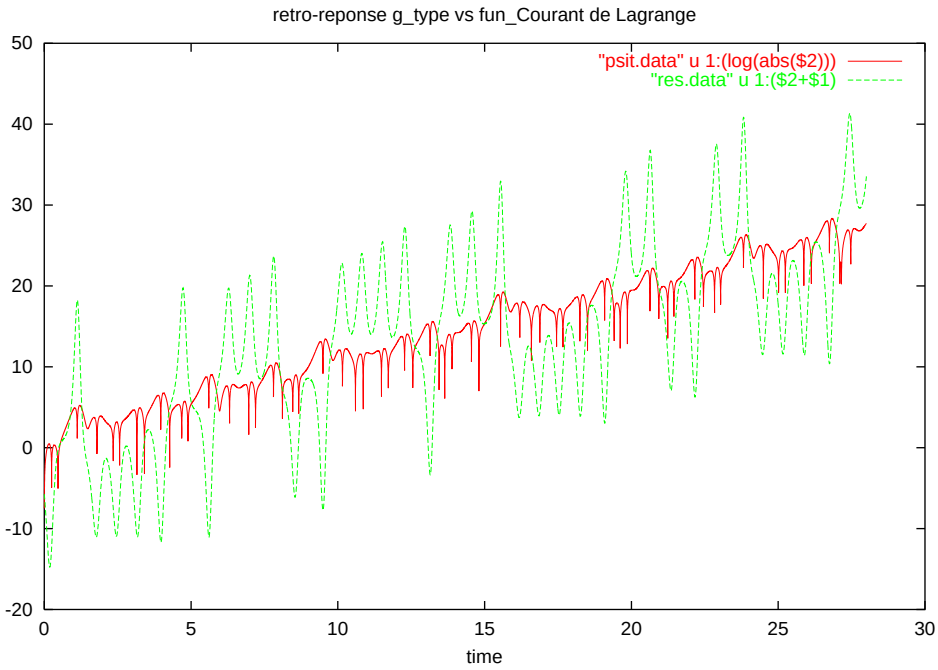

FIG. 2 – CTLS feedback-effect $\rho(0, \tau)$.

The log-scaled function clearly shows an average linear increase following the first Lyapunov exponent ($\lambda_L \simeq 0.95$), as well as the amplified zigzag preceding each transition (notice that the x axis has been rotated to follow the log-Lyapounov increase of the feedback function).

In comparison, the TLS-gain is the static function of the response-time to a step-perturbing function applied at a particular point of the trajectory (Fig.3) :
At every point of the trajectory can be defined an autonomous system and its response to perturbation. When this constant Jacobian matrices system is integrated in open-loop mode, the feedback-gain is obtained.

In Mini_ker, this function is automatically computed using the spectral decomposition described in the Letter.

One can notice that the TLS-gain always has real poles only, in three different shapes

– negative with finite asymptote, see points 2, 6, 10 ;
– negative runaways, see points 12, 14, 16 then 20 ;
– the preceding one finishing up a positive runaway sequence (18 and 19) ;

we shall see that the short positive sequence is a characteristic of an end of transition between the two wings of the attractor.

Stationary feedback-effect.

Contrary to the gain function, the feedback-effect shows oscillating sequences. This means that the chosen transfer variable is at the origin of the oscillation of the model, that disappears when the loop through this transfer is cut in the feedback loop.

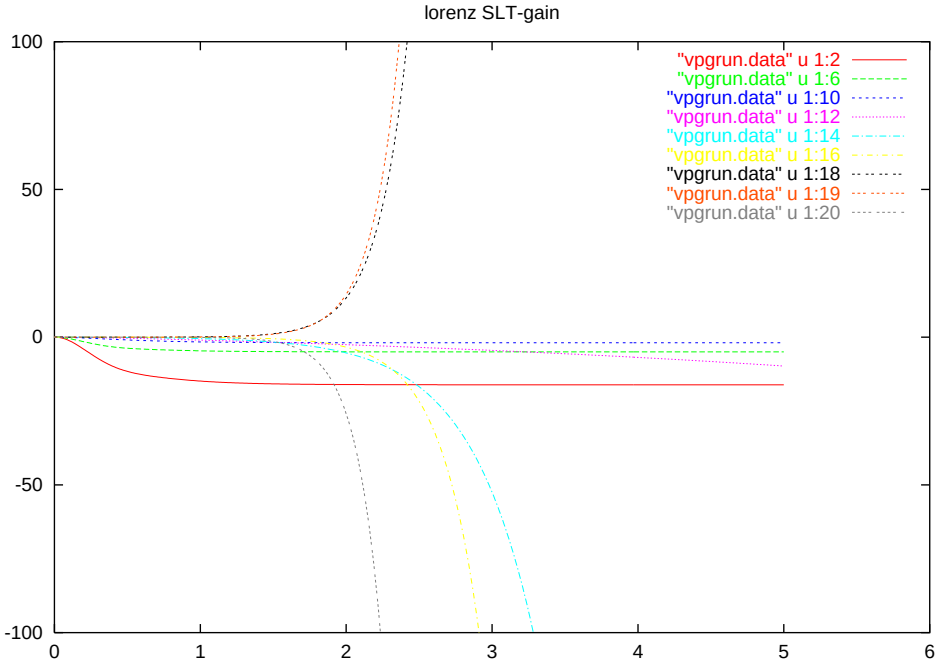

FIG. 3 – SLT-gain $g^s(t, t+\tau)$

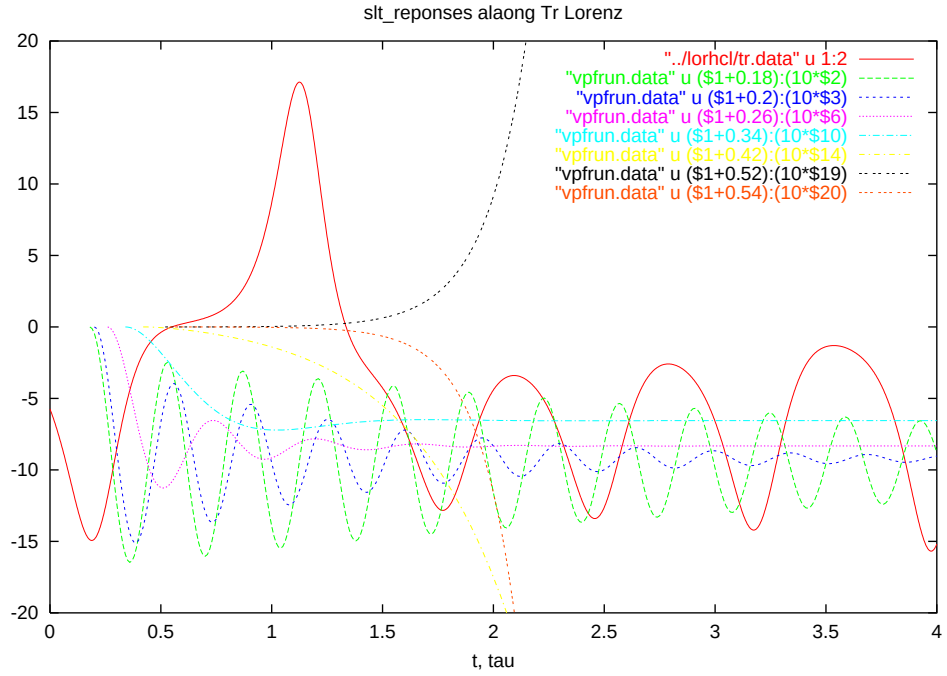

FIG. 4 – TLS feedback effect $\rho^s(t, t+\tau)$.

We now focus on an orbit (point A) first, and second when approaching, here a double transition (point B) along the trajectory (Fig. 5). Notice that we are here exploring a different trajectory than in the Letter.

On figure 6, we start at point A and examine a sequence of seven TLS-effect responses ; the perturbing step has an amplitude of 10 for clarity.

The first response is a weakly damped oscillation, followed in 2 by a large amplitude and large period oscillation ; the period goes next to its more current

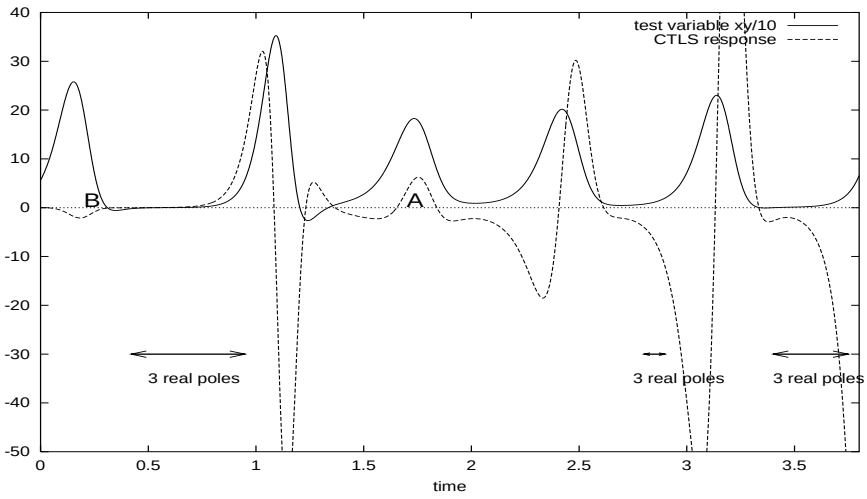

FIG. 5 – Portion of the trajectory.

value in 3, and goes back to damped responses at the remaining points.

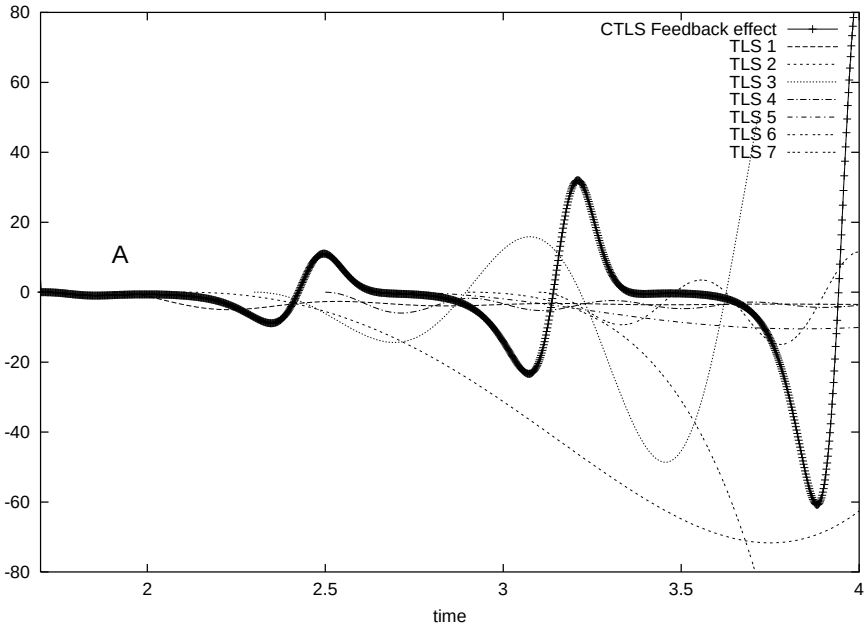

FIG. 6 – Orbits and CTLS feedback effect.

We can also look at the full sequence of the poles (fig. 7). What is shown are the feedback-effect Laplace-transform complex amplitudes, showing a systematic real pole and a complex conjugate pair possibly degenerating in two real poles. Now the

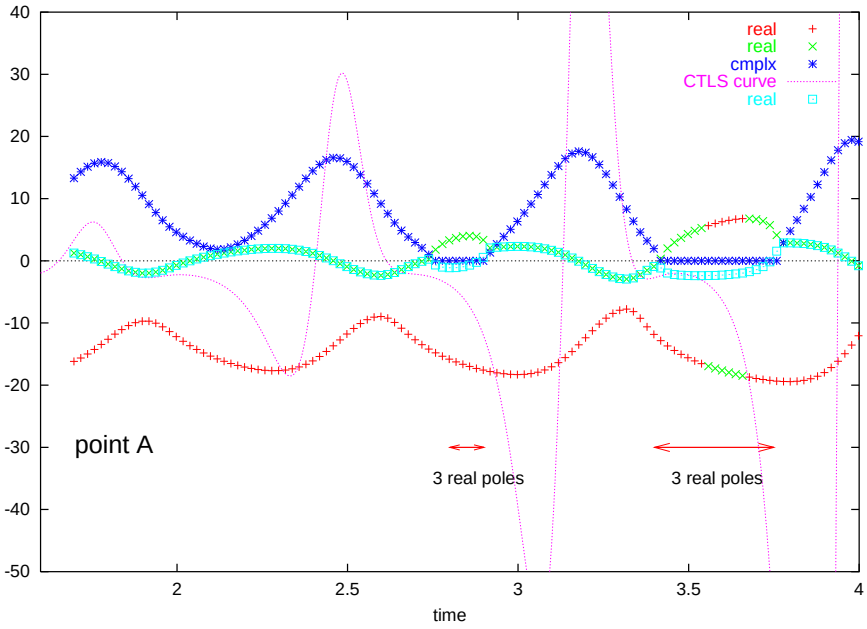

FIG. 7 – CTLS-effect and the population of TLS poles.

sequence along each orbit is quite clear : each orbit initiates an instable crisis that starts with a three-real poles sequence (3RP), followed by a diverging oscillation that becomes finally damped. The same full sequence is reproduced at each new orbit, except that the three-real poles sequence becomes longer, corresponding to the increase in amplitude of the CTLS-zigzag feedback effect.

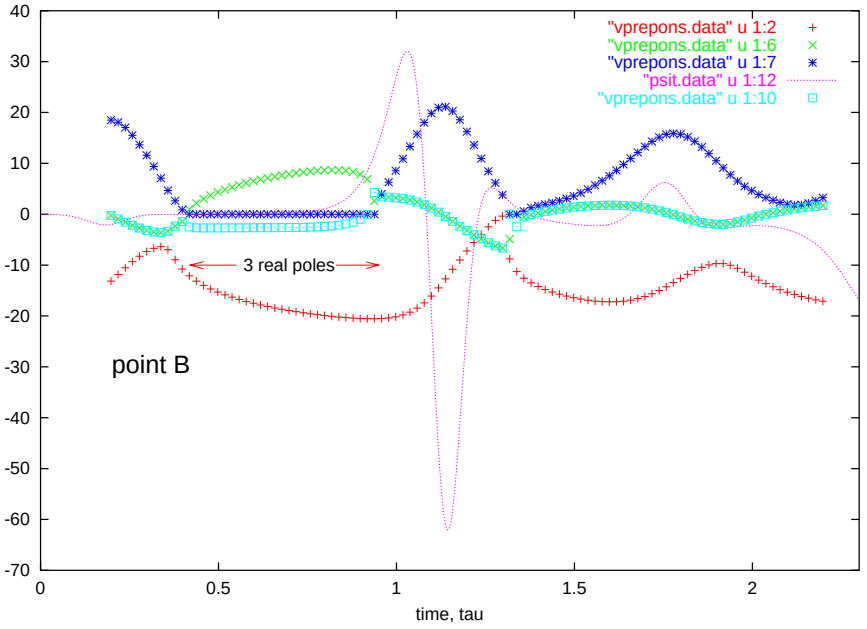

FIG. 8 – TLS feedback effect functions $\rho^s(t, t+\tau)$.

Figure 8 illustrates the same TLS poles population when approaching the

transition (point B). One can see how the oscillating sequence is replaced by three exponentials (one being unstable) ; then during the transition, the oscillations are retrieved that seem to allow the system to recover a new orbiting sequence, but now on the right wing.

1 Another portion of the trajectory (same as in the Letter)

Figure 9 shows the same part of the trajectory as the one of the Letter, with four orbits before transition. As already said in the Letter, the Lorenz system is symmetric across z, so that the $\varphi = xy$ variable is quite insensitive to the transition, whereas it is conspicuous in the CTLS feedback function.

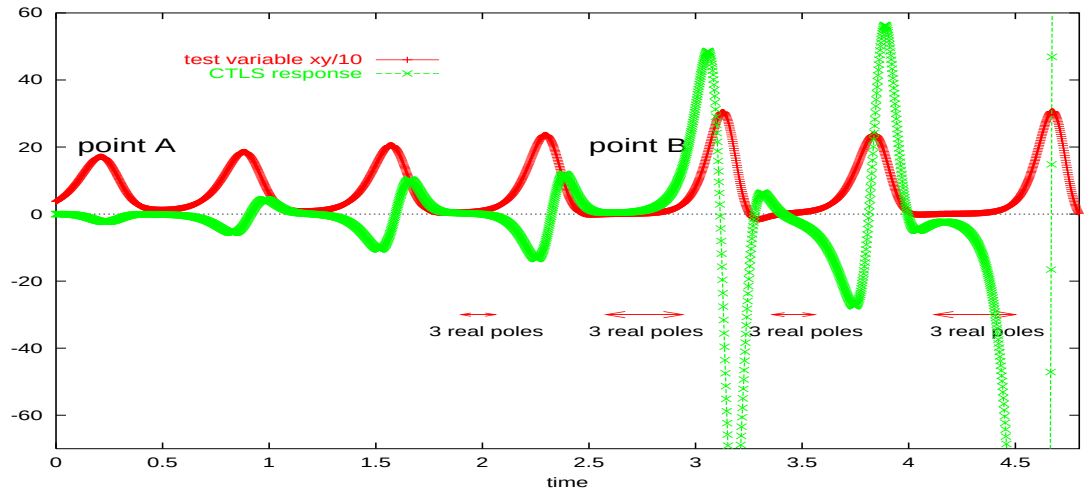

FIG. 9 – Test variable trajectory in the Lorenz model and Feedback Effect.

Between points A and B, $\varrho(t,0)$ shows oscillations of increasing amplitude, corresponding to the nonlinear instability of the system. The revolution around an orbit – one of the wings – involves "along" and "across" feedback effects in a zigzag shape. We call "along" a sequence when the feedback response is positive, because a positive perturbation in xy along an orbit can be considered as a force drawing the point toward or away from central point (0,0). When positive, the response is, roughly speaking, aligned along the perturbation. Conversely, a negative feedback effect means that the response is, roughly speaking again, perpendicular – "across" – to the perturbation, causing a rotational effect.

The four orbits show that the system reacts in the across way when heading to apogees (away from $0,0$), and in the along way when backing toward perigees (close to $0,0$).

The more distinctive feature is the change in sign of the CTLS zigzag just before transition : the *along* amplified reaction is now leading, followed by a strong *across* effect near the apogee, finally resulting in the leaving of the left wing for the other.

Figure 10 illustrates the long-term effect of the same function. For clarity in the collocation with transitions, the x variable is plot with a rotation to follow the Lyapunov increase ($x \to x + \lambda_L t$). The linear logarithmic increase is in average

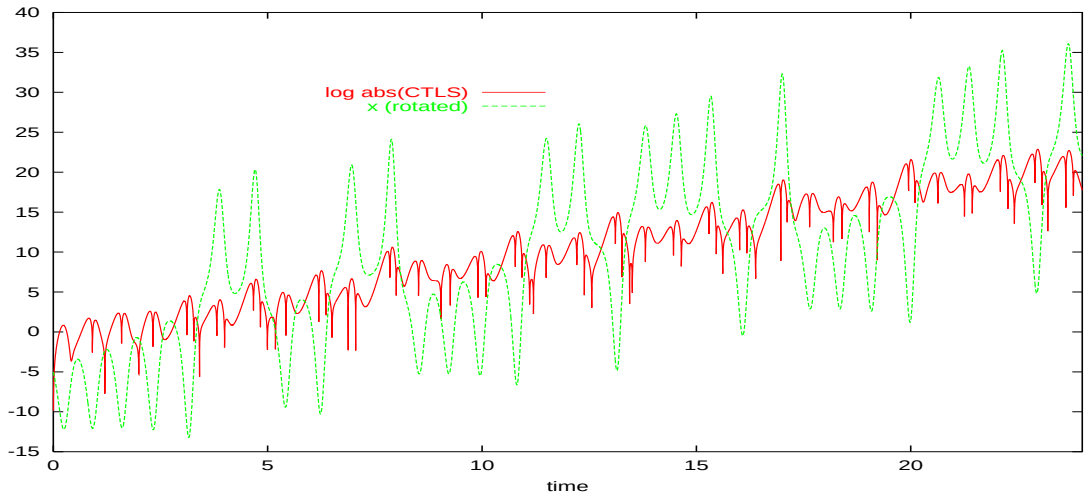

FIG. 10 – Long term feedback response (log scale) and x trajectory rotated along the Lyapunov exponent.

following the Lyapunov exponent ($\lambda_L \simeq 0.95$). More surprising is the similar increase of the zigzag amplitude.

The CTLS is clearly detecting the transitions, not only with an sudden increase in the zigzag amplitude, but also with a change of sign of the leading bump, now positive (fig. 9). We verified that among the different terms of the RHS of the system no other test variable is showing the same reverse in sign (see Fig.21).

Analysis of a trajectory starting far from the attractor.

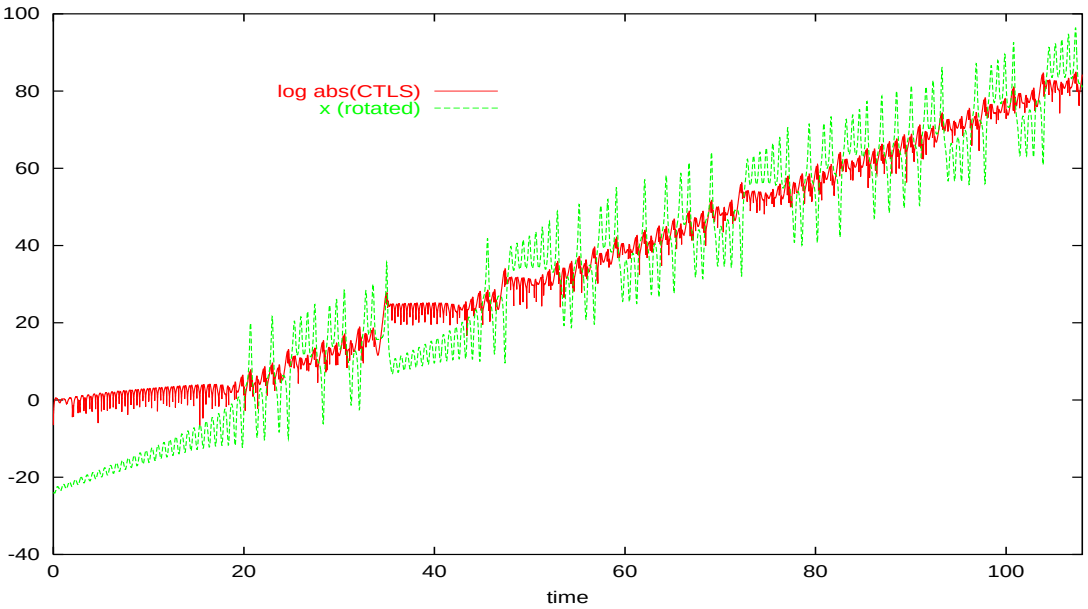

FIG. 11 – Same as fig. 10 with initial conditions out of the attractor.

Figure 11 is analog to Fig. 10 for different initial conditions, chosen far from the attractor – in fact, close to the point of no-convection of the left wing. It is noticeable that the CTLS-effect shows a weak increase when out of the attractor. That is observed each time the point leaves the attractor, see times : $35, 48$ et 73. Clearly, the attractor is exerting its effect by "stabilizing" - that is, decreasing the

exponential growing – when outside of it, compared to the asymptotic behavior as soon as the current point lies in the attractor.

These remarks are justifying the interest in the dynamics of the feedback functions, with a detection of transitions and a behavior depending on some "distance" to the attractor in the attractor basin. We will now consider the same functions at a closer look at the system dynamics.

A ZOOM on the orbits before a transition

Let now examine four orbits going to transition. On Fig. 12, the x, y trajectory is plot with error-bars, characterizing the CTLS feedback effect log-scaled. Error-bars are the CTLS amplitude (log-scaled), plot as vertical when above the mean Lyapunov increase (along effect, horizontal when under (across effect). Both orbits are followed clockwise.

The first orbit shows the *across* effect only, when the point is orbiting around the left-wing point of steady-convection (at center of orbits). Between point 1 and 2 on the fourth orbit, the point is decelerated toward perigee by the *along* reaction, then accelerated when heading to the apogee. This suggest that the *along* effect is caused by a repulsion from central point.

The transition is started by a strong *across* reaction after the apogee (5), and the circulating point is again decelerated by repulsion from central point, but with an offset that kicks off the point into the right wing. The end of the trajectory in the figure shows a strong *across* effect corresponding indeed to a just following second transition (not shown).

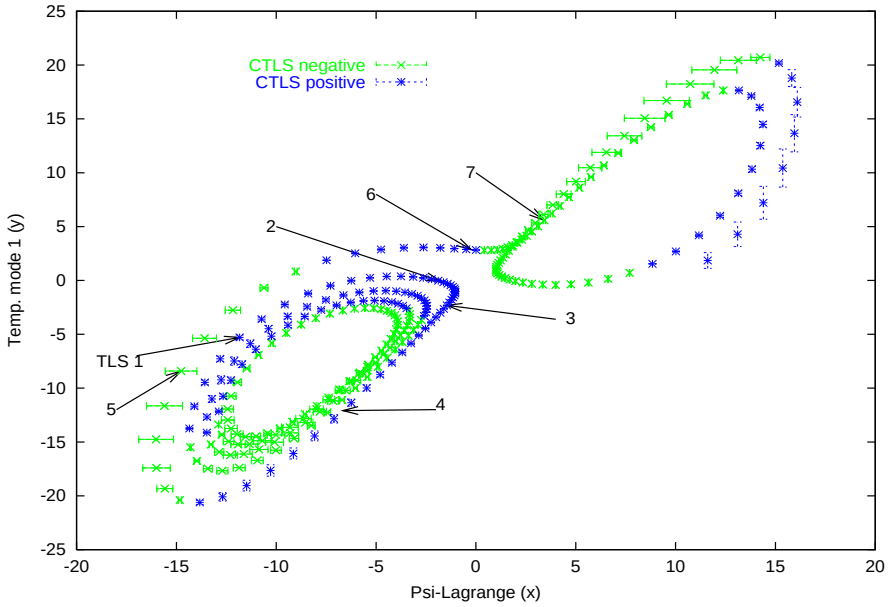

FIG. 12 – CTLS response before transition (scaled, see text).

Finally, the preceding analysis of the nonlinear feedback features of the model allow different interpretation, from global to close-up views, that in our belief totally justify the interest of computing such functions when a dynamical interpretation of the behavior of a system is needed. Notice that the present analysis is not based on physical interpretation of a feedback-loop structure at all. Of course, when

concerned with a physical process, the preceding interpretation is enriched with physical mechanisms expressing their dynamics.

1.1 Comparison with stationary feedback effect

Let now illustrate the connections between stationary and non-stationary feedback effects with two portions of the trajectory, looking at the complex amplitudes of ϱ functions in the Laplace domain. The elements of the spectral decomposition are double-scalar products $< c^{\dagger} \mid e_i >< f_i \mid b >$ in Eq. (9) of the Letter with $\tilde{u}(\mu) = \frac{1}{\mu}$.

Once a triplet of the model parameters is being given, one can imagine the state-space as filled with poles and associated complex amplitudes of the TLS-feedback effect – one can think of an analogy with Higgs bosons in the quantic vacuum. The non-stationary response builds up grabbing these elements along the reference

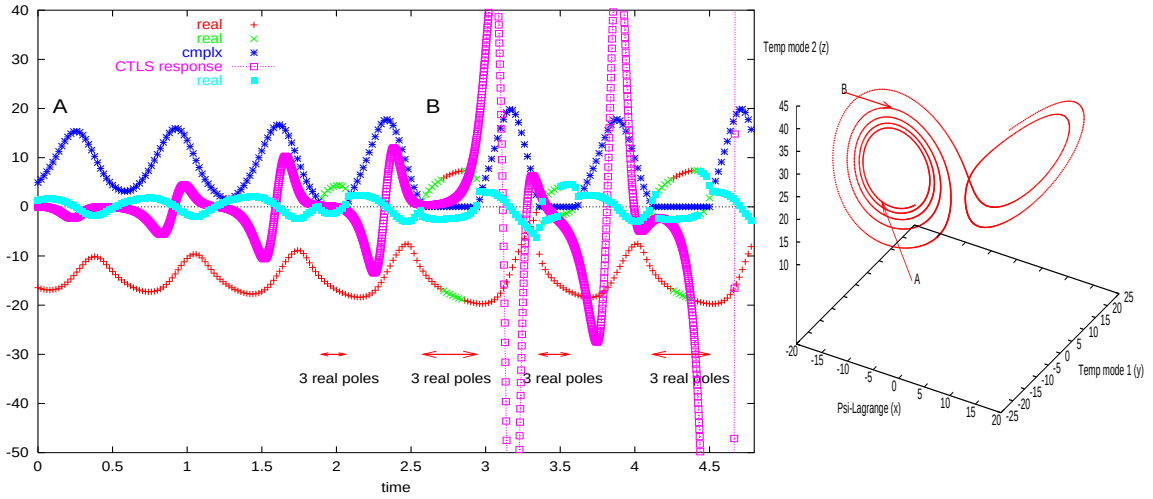

FIG. 13 – CTLS Feedback effect compared to TLS structure amplitudes.

trajectory. The way CTLS-functions build up is not intuitive – see the annex – because the state-transition matrix is an infinite product of elementary stationary ones.

Along the first revolution in Fig. 13, the non-zero complex amplitude is responsible for the *across* (or rotational) response of the CTLS-effect. This is followed by pure real amplitudes with an increasing trend. These are the "three real poles" sequences marked on the figure. The duration of that type of sequence regularly increases at each new revolution, until the transition phase is reached. After the transition, the 3RP sequence shortens, but does not cancel. In fact, the second orbit in the right wing leads to a new transition.

In the real space – that is, after inversion of Eq.(9) in the Letter, the stationary feedback function $\varrho^s(\tau)$ can be displayed as function of the response time τ, the point of the trajectory being the starting point of the step-perturbation applied ($\tau = 0$). In Fig. 9, the CTLS-effect is given once for all with a scaling by $\exp(-\lambda_L t)$. Each TLS ϱ^s function is similarly scaled by $\exp(-\lambda_L \tau)$.

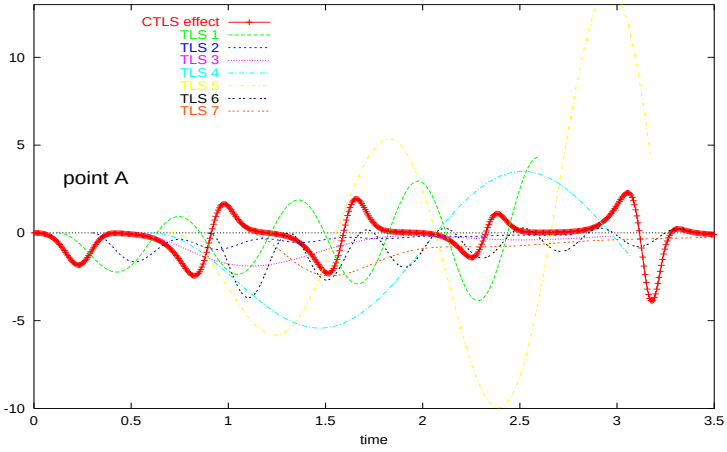

FIG. 14 – Different Feedback responses along two orbits after point A.

Figure 14 displays seven of those TLS-functions along the two first orbits (point A). The first shows an unstable oscillation with a period comparable with the CTLS double bump oscillation. Second and third TLS-functions are at beginning and end of a damped oscillation sequence with slowly increasing period. At point 4, the period is about four times greater than the shorter one, and ends with the flat portion of the CTLS response. Around TLS 5, a short sequence of unstable oscillation is preceding the rise of the CTLS zigzag. With TLS-(6) and (7), damped oscillations are recovered, announcing the following flat section of the CTLS.

It is remarkable how the nonlinear effects of the model are "absorbing" the unstable TLS-effects, but also remarkable is the non evidence of their relation. One can also remark that none among TLSs is able to give any good prediction of the true CTLS effect. It might be proposed to build a measure of the local nonlinearity of a system by giving a "time of prediction" within some upper bound of the TLS response.

Let now move to point B. Figure 15 shows some more TLS-functions along last orbit before transition. Notice that the CTLS has been restarted at point B, so that the change of sign of the zigzag preceding the transition has disappeared. TLS 1

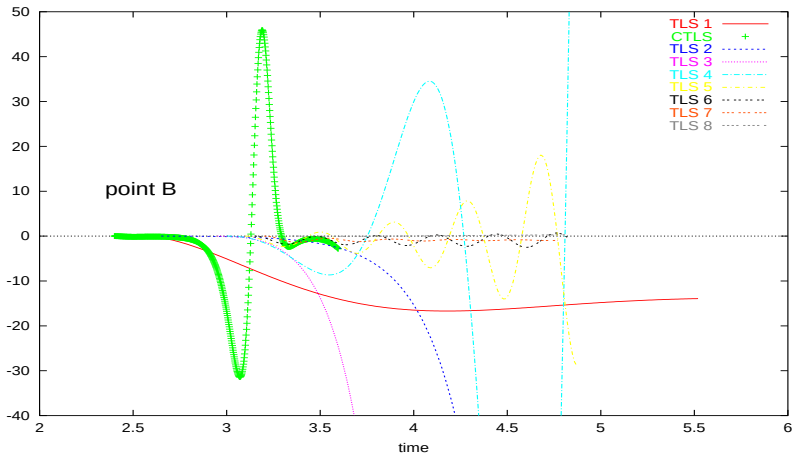

FIG. 15 – Across effect of TLS in approach to transition.

initiates a series of oscillations quite different than the one seen after point A. The first response – magnified by a factor of 10 for clarity – is converging to a negative

asymptote ($\varrho^s \to -0.8$), at the origin of the *across* effect of the perturbation on the system.

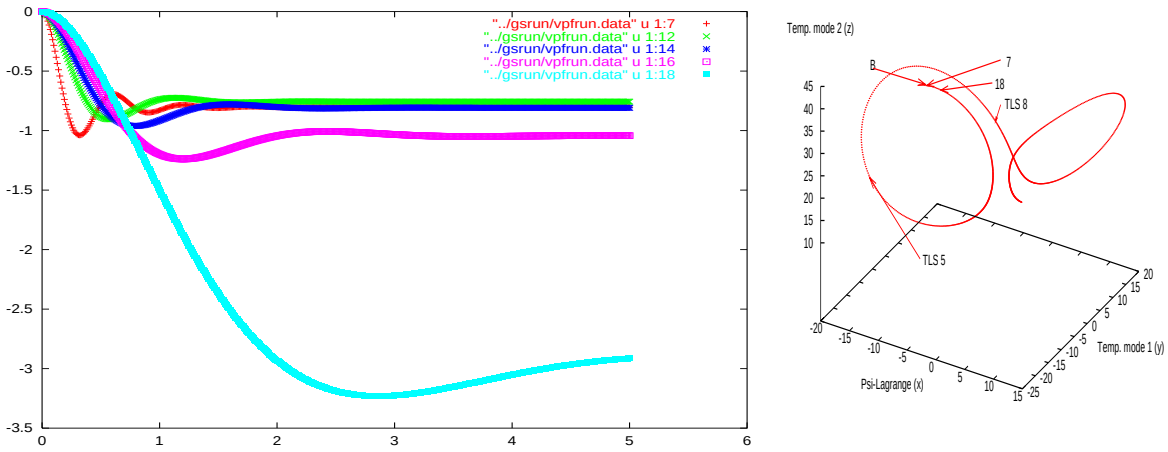

FIG. 16 – More explicit across-effect toward transition (TLS).

It is clearly seen with figure 16 how this rotative effect starts and amplifies. This effect is becoming divergent with TLSs 2 and 3, at beginning of transition. Then, return to unstable oscillations (4, 5), finally becoming stable from point 6. TLS-(7) response is also stable, whereas the last one shows a linear (scaled) instability. At this point, the transition to the adverse wing of the attractor has ended.

How does the system recovers from transition ? This is seen on Fig. 17. The end of

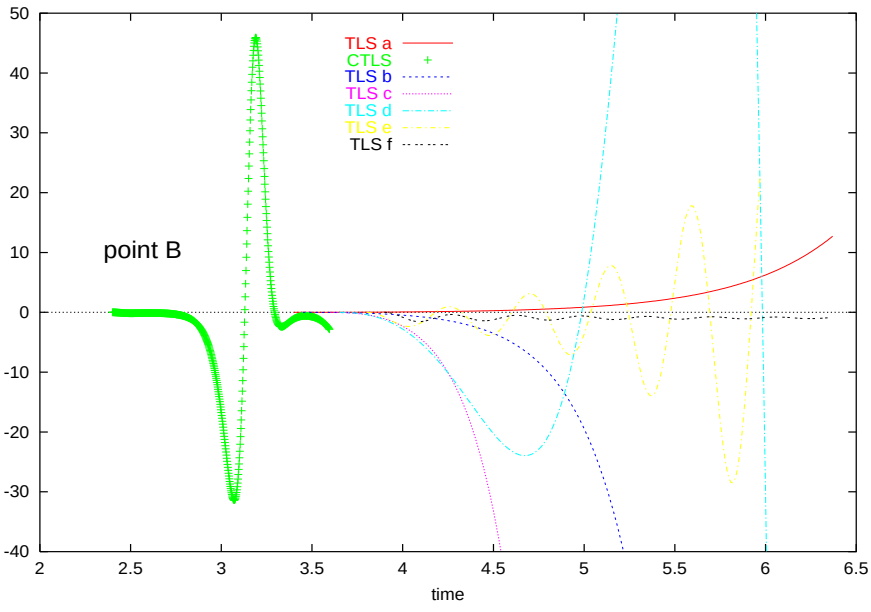

FIG. 17 – End of transition (TLS effect again).

transition is marked by TLS a of positive increase, that appears to be a characteristic of transitions in this system. Two *across* diverging TLS-effects then appear (b and c). Then the stationary tangent system responds with unstable oscillations (d and e), with growing periods, to back up to damped oscillations on the first right-wing orbit.

Link with the three poles sequences.

As figure 18 shows, the 3RP sequences correspond to *across* periods of the stationary feedback effect that becomes diverging. This suggest that the "rotating repulsion" by each point of no-convection is accumulating its effect orbit after orbit until transition. The last TLS (black curve) – just after the 3RP sequence – is

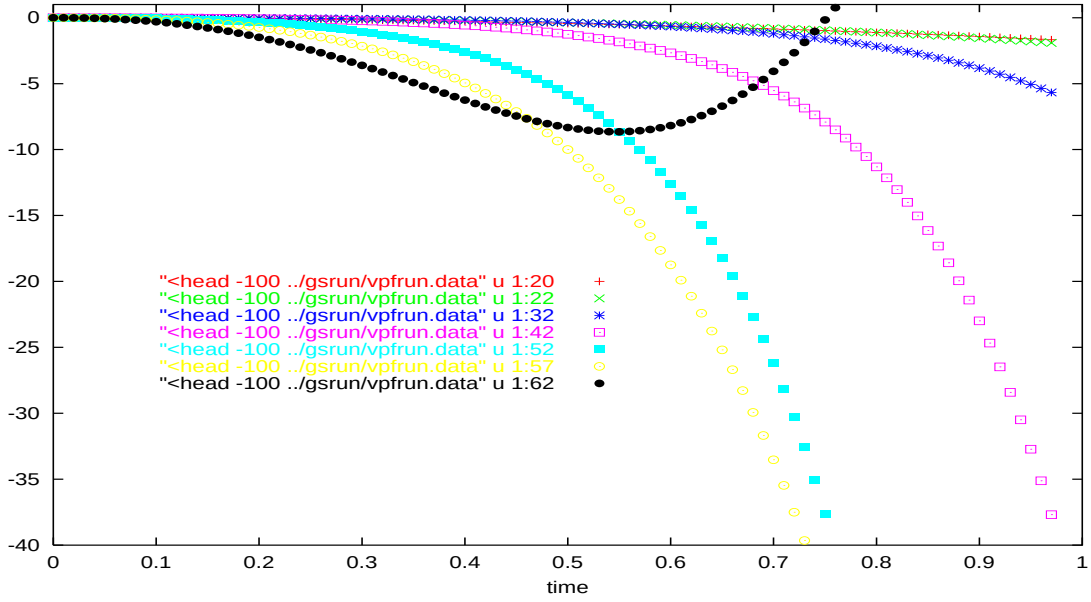

FIG. 18 – TLS-effect going to transition.

unstably oscillating at the beginning of the positive bump of the CTLS-effect.

A synthesis between SLTC versus TLS feedback effects.

Now, all TLS functions are systematically drawn along the four orbits trajectory (Fig. 19). The scatter plot shows the stationary feedback effect with the τ axis going down from the current point of the non stationary response. Due to the strong variation in amplitudes, the functions are scaled with a tanh function that keeps linearity of the response between -1 and $+1$, and where ± 2 represents infinite amplitudes. Thank to that scaling, one is able to follow the transformation of the periods in the oscillating sequences in particular.

Each revolution around an orbit shows the same type of sequence : when heading toward apogees, one meets exponentially growing amplitudes of oscillation with decreasing period until becoming close to the one of a CTLS zigzag. The oscillations then recover a relative stability when backing to perigees. Each new orbit just shows an intensification of the preceding features until transition. Along

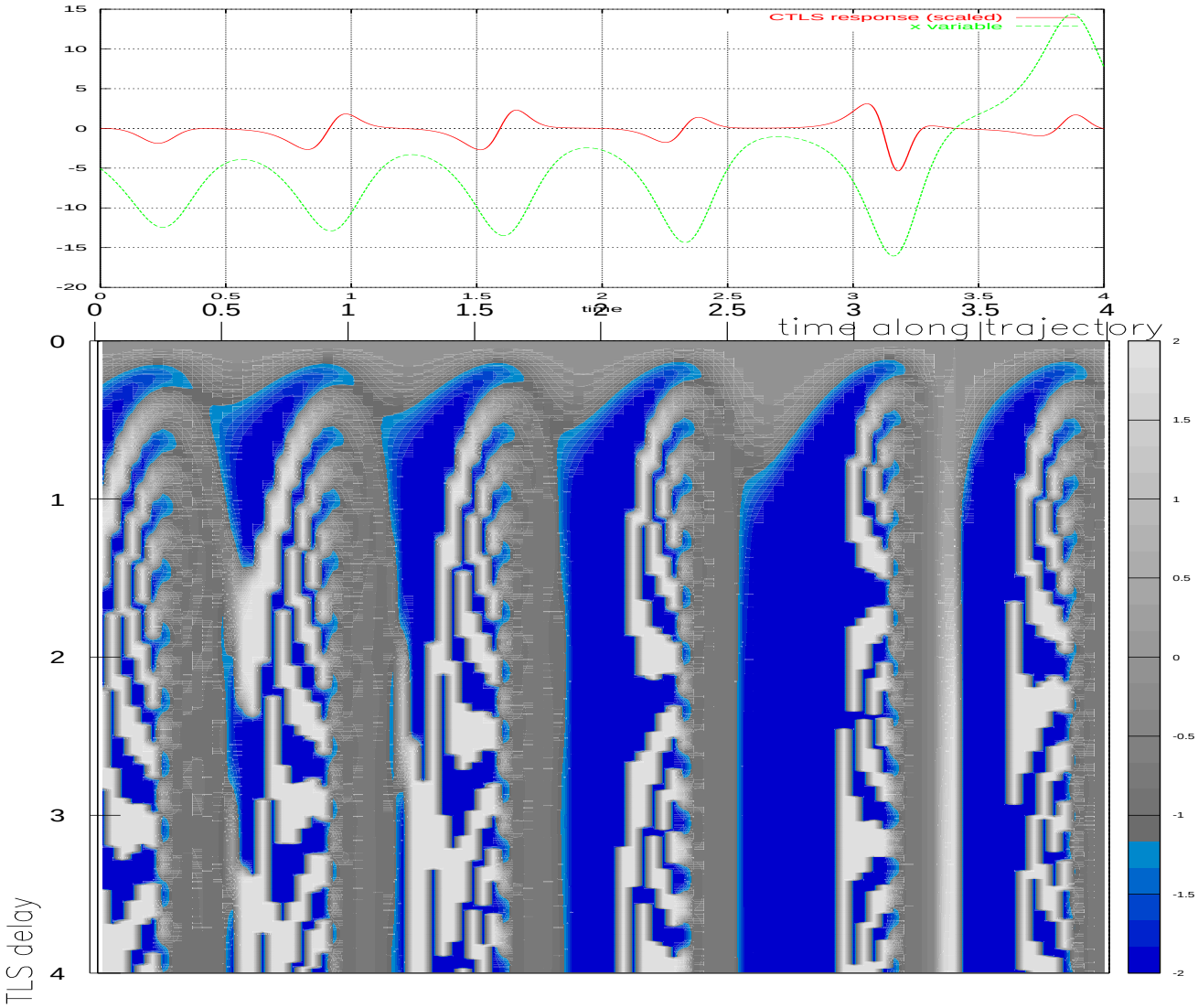

FIG. 19 – CTLS- and et TLS-effects along four orbits going to transition.

the four revolutions, one can observe the 3RP sequence as the blue vertical band : it corresponds with the *along* repulsive effect from central point that is found to increase also each new orbit. The white vertical band at approximately $t = 3.4$ is

the unstable exponential sequence characteristic of transitions. On the right wing, the tree real poles sequence is now reduced in duration but, as already noticed, is announcing a transition soon happening (not shown).

A synthesis between SLTC-effect and TLS-feedback gain.

Figure 20 shows the same synthesis, but now with the stationary feedback gain $g_s(\tau)$. The scaling is again in tanh, with linearity between -5 and 5, log-function out of this interval, and infinite in ± 10. The absence of oscillation is remarkable : in the open-loop mode, that is, when the $\varphi = xy$ "model" is not responding to the perturbed system, oscillations are suppressed. The only positive gain at $t \simeq 3.4$,

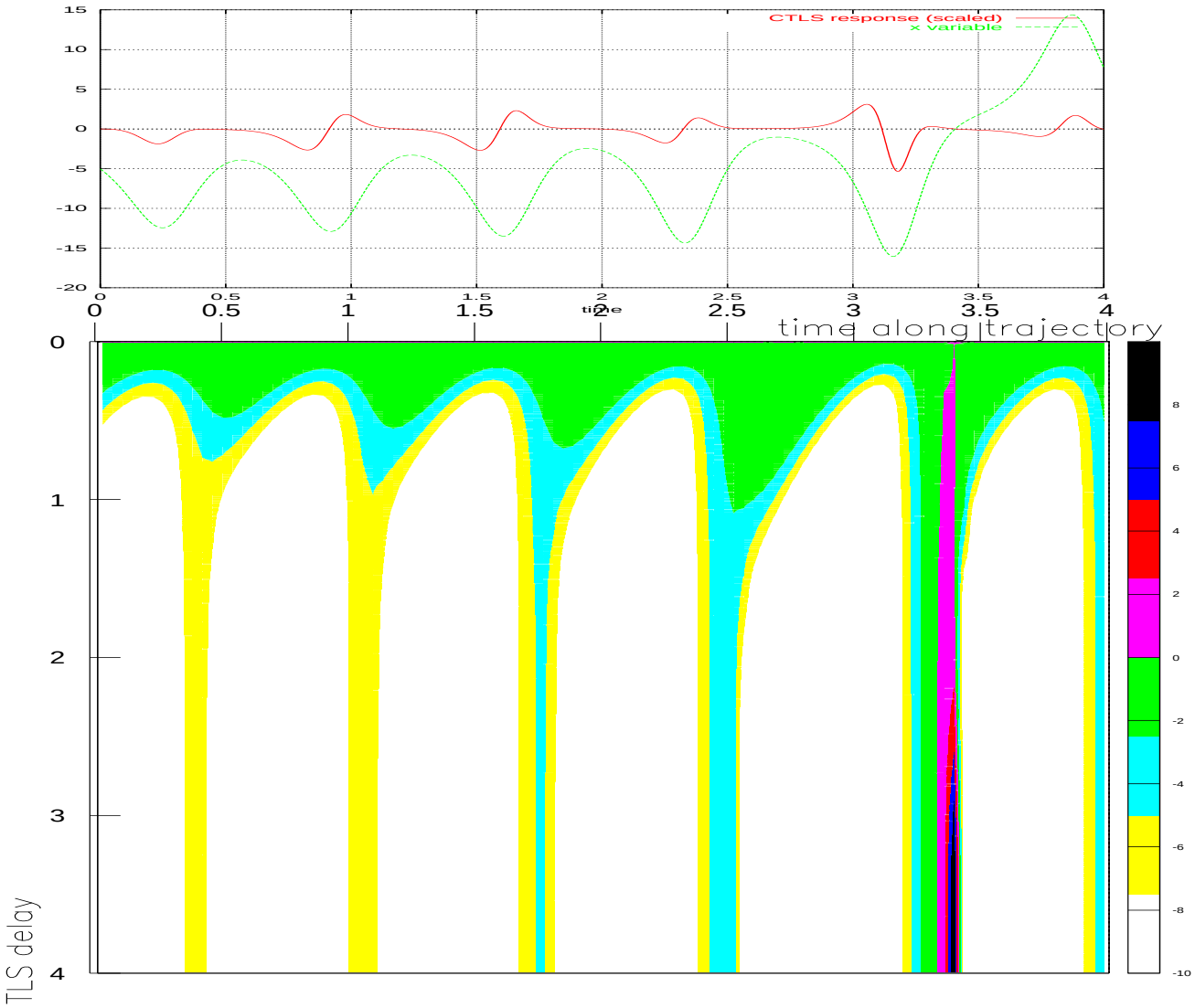

FIG. 20 – CTLS effect compared to TLS feedback gain $g_s(\tau)$ along the four orbits before transition.

is very short in duration at end of transition. One can notice how each rise toward apogee shows a very repulsive *along* gain with growing duration along the four orbits, whereas backing to perigee shows a decrease of it. Moderately negative sections of the gain-function are responsible for oscillations if the feedback loop is closed : $\dfrac{g}{1-g} = g + g^2 + g^3 + ...$, with powers understood as iterated convolution products.

CTLS for different test-variables

Figure 21 shows the CTLS feedback effect for test variable as copy of x and y, and a third one is xz, in addition to the previous xy. Same normalization and two first orbits. Copies are multiplied by 10. The same amplification of the zigzag is seen on all responses, but on the xy only is seen a change of sign before transition. Even

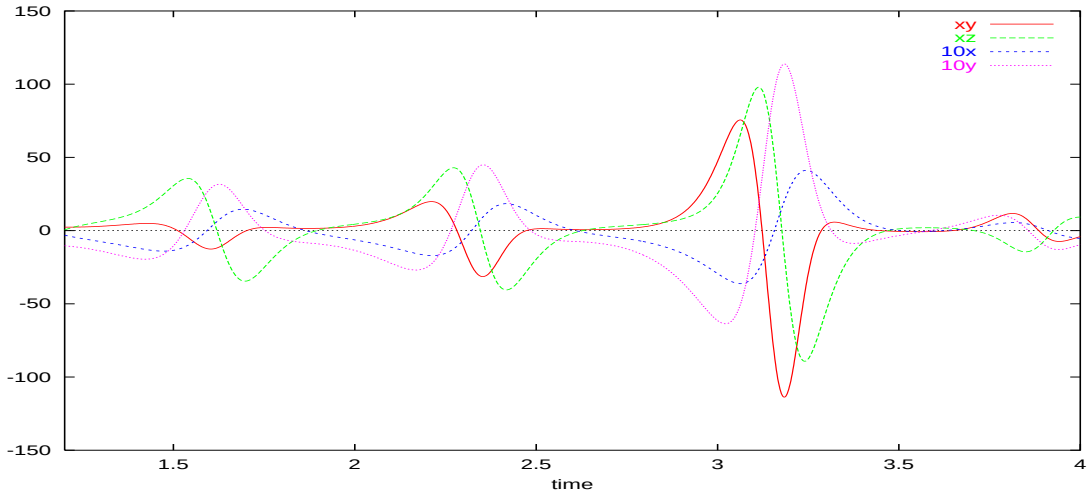

FIG. 21 – Comparison between four test-variables CTLS feedback effect function.

in a low dimensional model as the present one, the feedback functions can respond quite differently in spite of the simple feedback structure of the loop. But the heavy

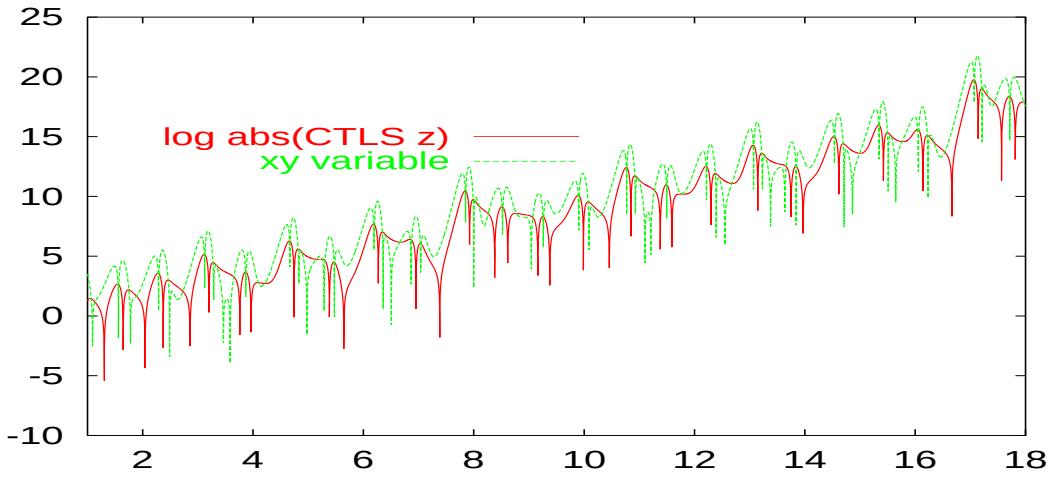

FIG. 22 – Comparison between long-term feedback effects for test-variables z and xy.

features, as here (Fig.22) the long-term Lyapunov increase, look similar.

Variable z is analyzed by Edouard Lorenz as the one that allows to follow the stability along trajectory and detect transitions. We compare that variable with the $\varphi = xy$ one (Fig. 22). One can see how they are giving the same type of information, this being understood looking at system (1), because z is exponentially converging to instant values of xy – as it will be detailed in the next section.

Essai of physical analysis of the feedback results

First consider transfer xy. A perturbation is applied to this interaction between speed of flow (in terms of a stream function mode) and the temperature difference between ascending and subsiding fluid particles. When positive, the perturbation intensify z, the difference between upper and lower fluid temperatures. This correspond to the speeding up of the flow that tends to depart low and up temperatures from the mean – taken in the Rayleigh-Bénard theory as the constant gradient line between limiting boundary conditions in temperature. As a result, the heat flow between fluid and surfaces will increase, thus fighting against the horizontal temperature difference y. That last parameter will thus decrease on the left wing (where x is negative). Because that horizontal gradient is the engine of the rotating of the fluid, the fluid vorticity will decrease. Finally, xy will decrease, hence the linear stability observed in the short-term..

General synthesis of the analysis

One can justify after the present study a "feedback" view on the Lorenz system based on three distances :

- as viewed from far enough, the attractor is playing its "attraction effect" by decreasing the local Lyapunov exponent ;
- going closer looking at a leaf, the change of sign in the CTLS zigzag announcing transition is linked with a repulsive effect from central point, after an intensification of the rotational effect induced by no-convection points ;
- getting closer again, each orbit shows a repulsive effect that cast the movement toward apogees, then followed by the rotational effect from no-convection points. It is only after numerous orbits are followed that the accumulation of the double effect swings out the movement to the adverse leaf ;

Knowing that the system is chaotic, it is not surprising that the CTLS function exponentially grows. What might be more surprising is that the log-scaled function looks quite independent of the starting point, and that the Lyapunov increase is immediately seen. What is changing with the starting point is the time where the zigzag is changing sign before a transition. This should be analyzed in more details.

Nevertheless, the interest of being able to analyze the CTLS feedback functions looks quite obvious for more general systems too complex to be considered from their equations. Also, when considering the numerous diverging log-scaled linear feedback effect functions along the trajectory, the CTLS instability is keeping its exponential increase, showing how the nonlinearities in the model are damping the linear instability.

As a final remark, the linear increase of the dynamical features once log-scaled suggests that an analysis of this system "a la Floquet" might be able to zoom on the detailed dynamical features of the model.

1.2 A numerical analysis of the open-loop system

Contrary to the preceding studies based on the tangent system analysis, we have also run the model in the open-loop mode, that is freezing the test-variable φ at some initial value, say d. In that case, the system linearizes quickly after z exponentially converging to $\frac{d}{b}$. Hence, once $z = c^{cste}$, the rest of the system is linear (see Eq. 1). As Edward Lorenz explains in his 1963 paper, there are transition values of z that we should verify numerically.

When starting from a point on the studied trajectories and a moderate value $\varphi = 100$, the open-loop trajectory (Fig. 23) is converging to the central point after an incursion to the right leaf.

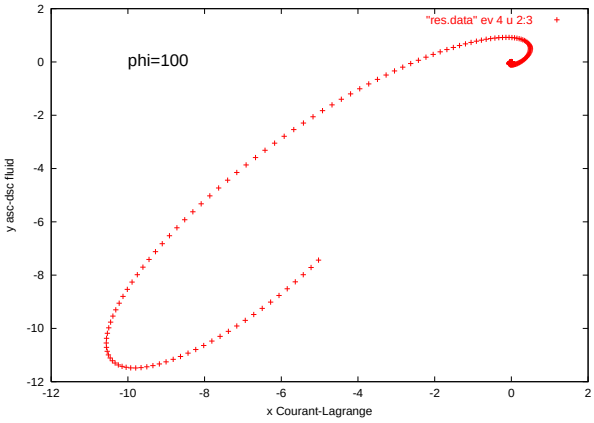

FIG. 23 – Lorenz model in open-loop mode, φ frozen at 100.

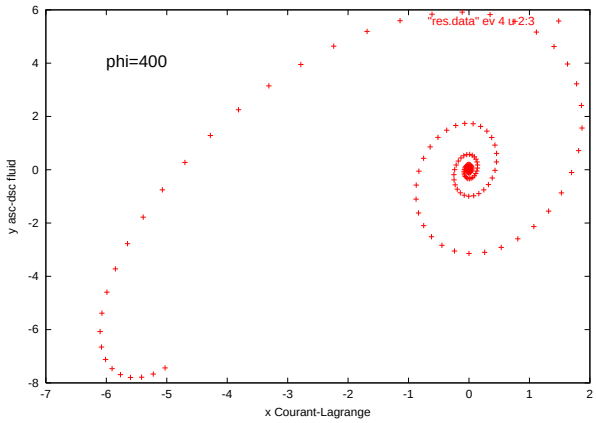

FIG. 24 – Lorenz with φ frozen at 400.

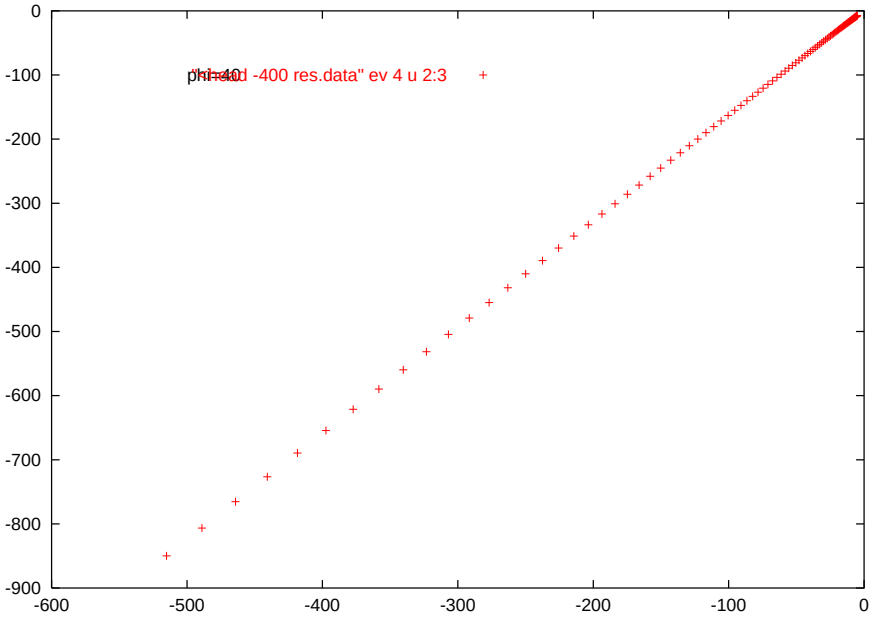

FIG. 25 – Lorenz with φ frozen at 40.

The greater value of $d = 400$ leads to an increased rotating effect both within the left wing and after transition to the right wing before converging to central point. For

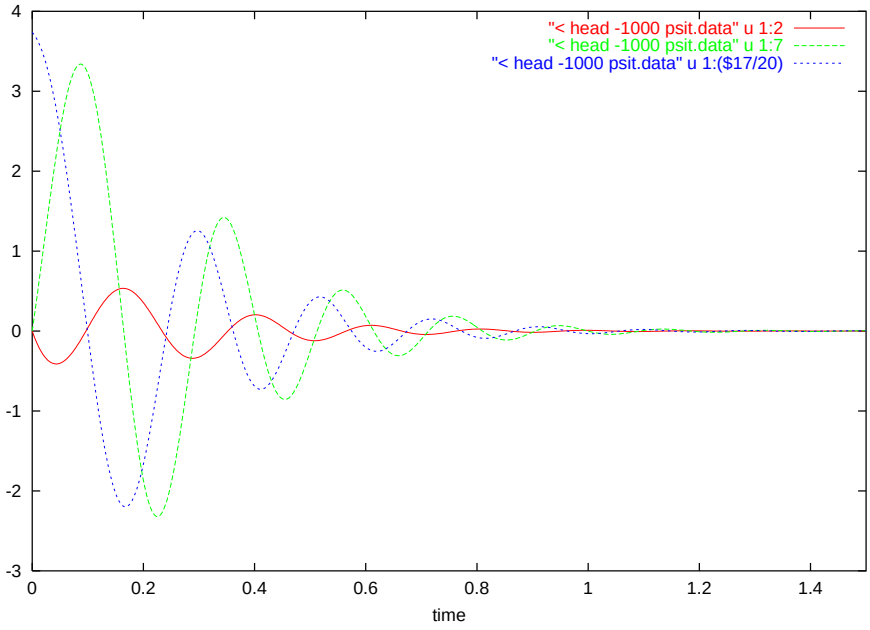

FIG. 26 – SLTC for different test-variables :2=x,7=y,17=xz with frozen $\varphi = xy = 400$.

a smaller value of $\varphi = 40$, Fig. 25 shows an exponential repulsion from central point, with a slope of approximately 2, that makes the movement not passing through the left no-convection point. This shows another transition between repulsive and rotating effects,. This justifies how the CTLS reacts along the four orbits as we interpreted it.

Coming back to the value of 400 that leads to a strong rotating effect, we now look at the CTLS effect on two other test-variables, the one copying x and y, as well as the xz one. Figure 26 shows indeed damped oscillations as soon as xy is frozen. This **is not** in contradiction with the absence of oscillations in the feedback gain response, because on the contrary, oscillations are seen until the system becomes linear, whereas by construction the TLS functions are linear responses.

1.3 Analysis of CTLS at fix points

Left point of no-convection (NC)

When system is positioned initially to the left point of no-convection ($x = -6\sqrt{2}, y = x, z = 27$), it responds to a perturbation with a divergent oscillation that corresponds to the instability on that point (Fig. 27) – with our set of parameters values. Consider the trajectory of CTLS effects on x and y as test-variables of

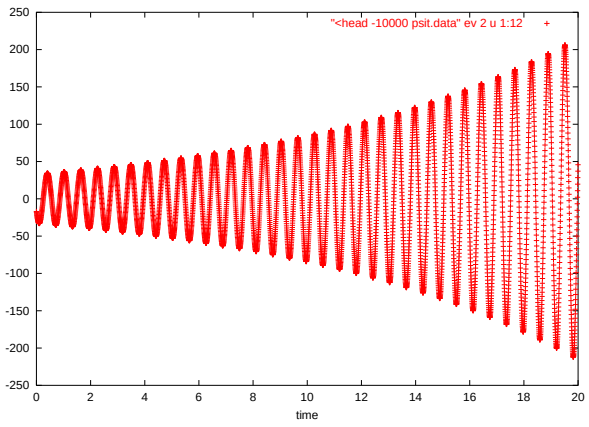

FIG. 27 – CTLS effect on variable : 12=xy at left point of no-convection.

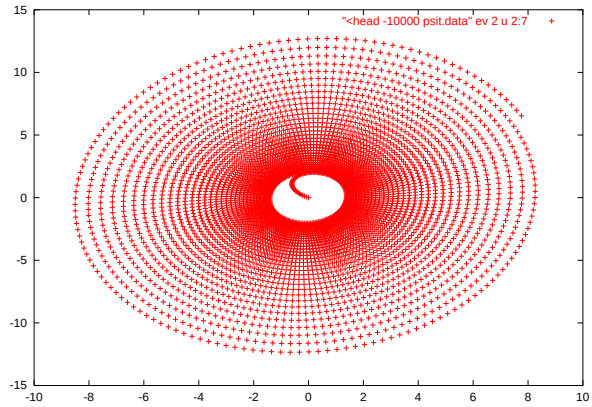

FIG. 28 – SLTC :2=x versus 7=y at left NC point.

Fig. 28. One can clearly observe that the NC point is causing a repulsive effect on both variables together with a rotational effect.

The exponential growing of the radius is seen on figure 29 (log scaled), with

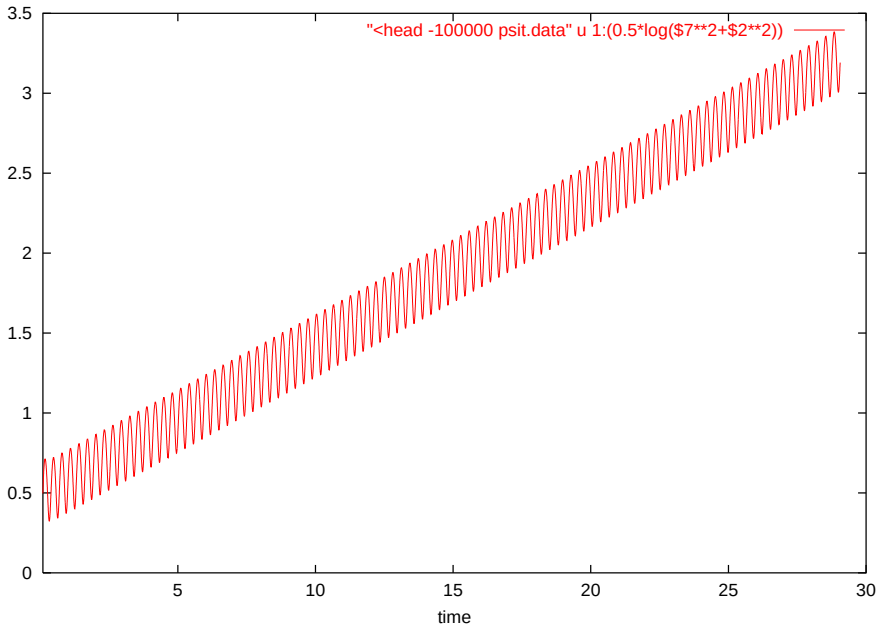

FIG. 29 – SLTC :x versus y at left NC point, log-scaled radius.

the value of 0.95 of first Lyapunov exponent, which justify our conclusion about an "orbital neutrality" along the Lyapunov.

Central point

Let now move the initial point to central point (0,0). There is no more rotational effect, replaced by a purely repulsive effect, passing far from the NC point (point C on Fig. 30).

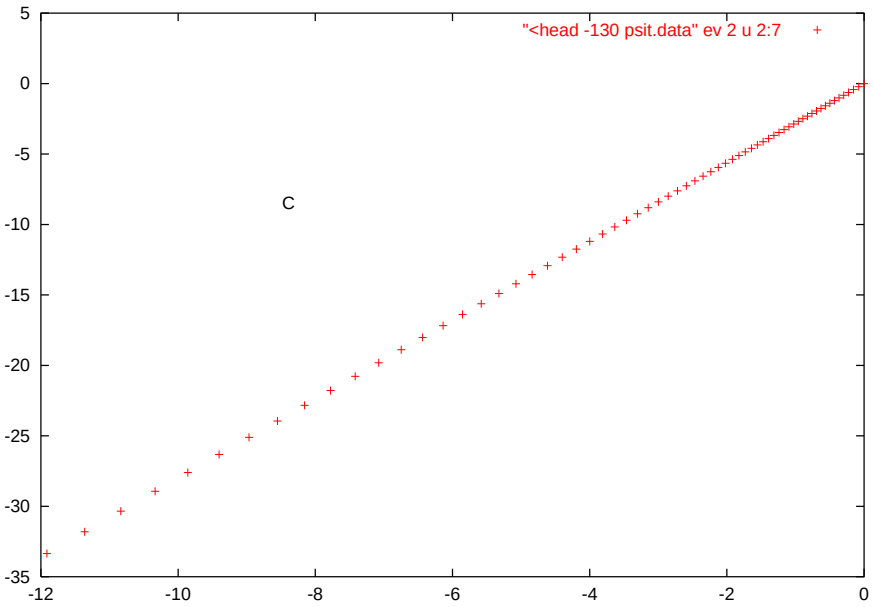

FIG. 30 – SLTC : x versus y at Central Point.

Annex : Linking TLS and CTLS feedback functions

How does the stationary responses combine in the true CTLS one ? Let consider a section of the trajectory from t to $t+\delta t$

$$\begin{aligned}
\rho_g(t+\delta t,s) &= < c^\dagger(t+\delta t) \mid \int_s^{t+\delta t} \Phi(t+\delta t,\tau) \mid b(\tau) > d\tau \\
&= (< c^\dagger(t+\delta t) \mid - < c^\dagger(t) \mid + < c^\dagger(t) \mid) \\
&\quad \left[\int_t^{t+\delta t} \exp(A(t+\delta t-\tau)) \mid b(t) > d\tau + \int_s^t \Phi(t+\delta t,\tau) \mid b(\tau) > d\tau\right] \\
&= (< \Delta c^\dagger(t;dt) \mid + < c^\dagger(t) \mid) \qquad (2) \\
&\quad \left[A^{-1}(I-\exp(A\delta t)) \mid b(t) > +(I+A\delta t)\int_s^t \Phi(t,\tau) \mid b(\tau) > d\tau\right]
\end{aligned}$$

The factor to $< c^\dagger(t) \mid$ in the bracket is composed of a first term that represents the stationary feedback effect function : $\rho_g^s(\delta t)$, and a second that, with the unit matrix of the infinite series of $\exp(A\delta t)$, is the CTLS effect : $\rho_g(t,s)$. Hence, at first order and at constant $< c^\dagger \mid$, the CTLS is built additively from the stationary effect function, with an additional term in δt :

$$\rho_g(t+\delta t,s) \overset{(1)}{\simeq} \rho_g(t,s) + \rho_g^s(\delta t) + < c^\dagger \mid A\delta t \int_s^t \Phi(t,\tau) \mid b(\tau) > d\tau \qquad (3)$$

This in particular is the full construction of the CTLS effect when the test variable copies one of the state variables – $< c^\dagger \mid$ is then the transpose of one from Euler basis vectors of the state-space.

More generally, the non constant $< c^\dagger \mid$ is responsible for the supplementary contribution

$$\begin{aligned}
+ &\overset{(2)}{=} < \Delta c^\dagger(t;dt) \mid \left[A^{-1}(I-\exp(A\delta t)) \mid b(t) > +(I+A\delta t+...)\int_s^t \Phi(t,\tau) \mid b(\tau) > d\tau\right] \\
&\simeq < \Delta c^\dagger(t;dt) \mid \int_s^t \Phi(t,\tau) \mid b(\tau) > d\tau\,,
\end{aligned}$$

taking δt such that $< \Delta c^\dagger(t;dt) \mid \sim \delta t$.

Finally at first order :

$$\rho_g(t+\delta t,s) \overset{(1)}{\simeq} \rho_g(t,s) + \rho_g^s(\delta t) + < c^\dagger(t)A(t)\delta t + \Delta c^\dagger(t;dt) \mid \int_s^t \Phi(t,\tau) \mid b(\tau) > d\tau \qquad (4)$$

In conclusion, and even when $< c^\dagger \mid$ is constant, there is indeed an immediate additive contribution of TLS to CTLS function, but it has to be completed by a cumulative effect depending on the preceding trajectory. The relative importance of the two contributions is depending on the system, and difficult to infer. Coming back to our proposition to measure nonlinearity with the predictive ability of the TLS, one could define the horizon δt such that the integral term in (3) is bounded.